Ion Conveyor

N. Joshi [a,1,*], M. Brodeur[b]

[a] *IAP, Goethe University, Frankfurt am Main, Germany.*
[b] *University of Notre Dame, Notre Dame, IN, USA*

Abstract

An Ion Conveyor driven solely by travelling waves is investigated for possible applications in low energy beam transport at various accelerator-based facilities dealing with thermalization and extraction of fast isotopes. In this paper, the simulation results for the transport of various isotopes through an optimized Ion Conveyor operable in the presence of moderate buffer gas pressure and homogeneous magnetic field have been presented. A short device is produced and experimentally tested for the transport of Rb^+ ions in the presence of gas pressure.

Keywords: `Ion conveyor, Ion guide, Low energy ion transport, Traveling wave ion transport`

1. Introduction

The Ion Conveyor is an ion guide device composed of multiple stacked rings. This kind of ion guides has previously been used in different configurations. A stacked ring RF device was first introduced by Bahr, Gerlich and Teloy in 1969, and later proposed by Guan and Marshall to be operated along with electrostatic potentials [1, 2]. Smith et al. used an ion funnel with a focussing effect to operate in the pressure regime of $0.1 - 40$ hPa, for experiments in 2000 [3, 4, 5]. Later in 2004, Colburn et al simulated the device operated with travelling waveform and also named it, "Ion Conveyor" [6].

*N. Joshi
Email address: `email@ninadjoshi.de` (N. Joshi)

An ion conveyor driven solely by a travelling wave, conceptualize by G. Bollen [7], is investigated for possible applications in low energy transport for radioactive ion beams. As shown in Fig. 1, the ion conveyor is comprised of a set of ring electrodes, connected to a signal generator with multiple output signals, shifted by equal phases, applied to the periodic set of electrodes. This arrangement induces a travelling wave along the structure. An ion "riding" on the wave is then pushed forward, the movement is known as "ion surfing", similar to the one used in RF-carpets techniques [8, 9, 10, 11].

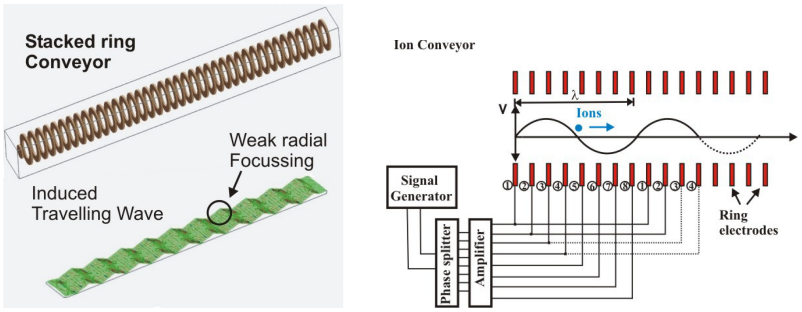

(a) (b)

Figure 1: Ion Conveyor: a) Ring electrodes are stacked; when connected to a signal generator, a travelling electric field is induced. b) The consecutive rings are connected to a signal generator with phase difference and the number of electrodes with a different phase defining a period.

Fig. 2 shows sample trajectories for three different cases. The first and second pictures compare the trajectories of Rb^+ ions at low amplitude wave and high amplitude wave. The trajectories in the top picture show the "Conveyor mode" in which the ions are carried along with the wave relatively slow. When higher wave amplitude is applied, the ions can be driven at faster speeds and a lower Time of Flight (TOF) can be achieved. This mode is called "Ion Squeezing" mode, which also exhibits a stronger radial focussing from the structure. The bottom figure shows Ar^+ ions with mass m = 40 transported through a conveyor in the presence of a magnetic field induction of 1.0 T in longitudinal

z-axis.

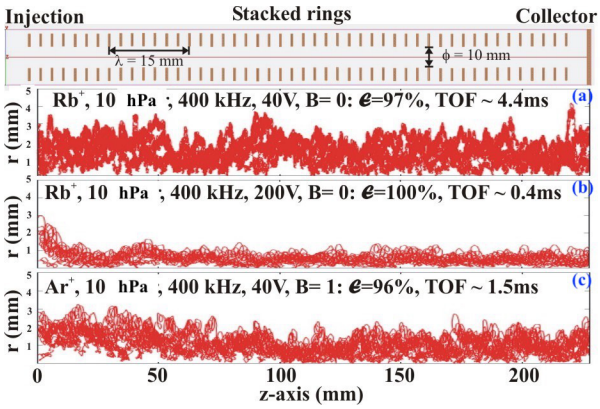

Figure 2: Sample trajectories of ions transported through Conveyor. a) Conveyor mode: Rb^+ ions in 10 hPa with a low amplitude sine wave (40 V), b) Squeezing mode: Rb^+ ions in 10 hPa with a high wave amplitude of 200 V, and c) Conveyor mode: Ar^+ ions in 10 hPa with a magnetic field induction of 1.0 T defined in longitudinal z-axis.

2. Simulations: Tools and Setup

The particle dynamics was simulated using two packages, namely SIMION and IonCool [12, 13]. SIMION was used to calculate electric fields from the given geometry of the conveyor. Then the electric fields were loaded into the IonCool package. The IonCool package calculates the motion of ions in the presence of arbitrary electric and/or magnetic fields modelling the effect of the buffer gas by realistically simulating collisions between ions and buffer gas molecules. Fig. 3 shows a typical geometry for the simulation of ion dynamics in the stacked ring structure in a two-dimensional projection. To isolate the problem of transport ions only through the structure and avoid any effects arising due to fringing fields, the thermalized ions are initialised a few mm inside the structure. This scenario is well suited to investigate the properties of ion conveyor alone. In the section 5 the optimized structure is simulated with the experimental setup.

The efficiency is measured by counting the number of ions reaching the collector plate downstream.

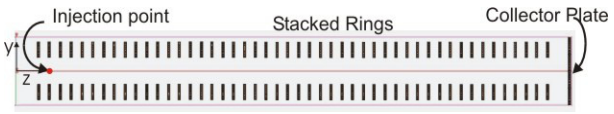

Figure 3: SIMION geometry model of ion conveyor. The initial injection point is located inside the ring structure approximately at the position of the second ring electrode. Efficiency is calculated by taking the ratio of number ions reaching the collector plate to the number of ions injected. The outer boundary indicates the simulation model limits.

The parameters which were varied for optimizing the structure were:

- Spacing between electrodes
- Wave Amplitude (defined as peak amplitude)
- Frequency
- Diameter of rings

3. 4-phase vs 8-phase and Square wave-based travelling wave

The initial assessment showed that a travelling wave generated with a higher number of phases benefits the ion transport not only in terms of the operating pressure range but also in terms of Time of Flight through the structure. The travelling wave is induced along the structure by superposition of the sinusoidal signal with a phase difference in the consecutive electrodes connected in a periodic set. Densely packed ring electrodes would produce a smoother wave as compared to the stepwise approximated travelling wave.

Fig. 4(a) distinctly shows that 8-phase driven conveyor can support a wider gas pressure range, whereas the Time of Flight (TOF) is also shorter for 8-phase structure as seen in Fig. 4(b). A higher number of phases like 16 or 32 would be

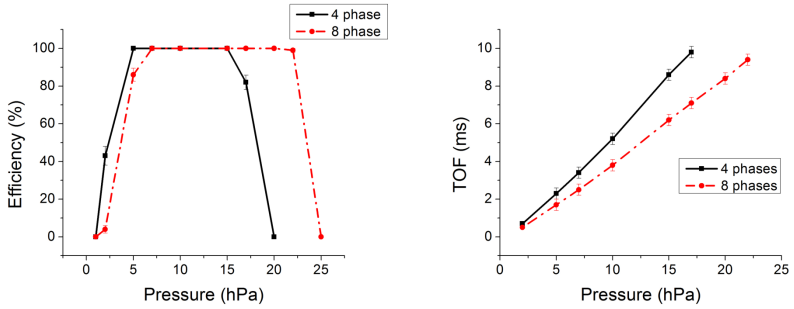

(a) (b)

Figure 4: A comparison between conveyor with 4−phases and 8−phases. An example of Rb^+ ions in 10 hPa with a wave amplitude of 40 V (a) compares the pressure range supported by the structure in terms of efficiency, whereas (b) compares the TOF as a function of pressure.

more effective, but also more challenging to handle from a manufacturing and operation point of view.

It was further shown that a travelling wave induced by square-wave can be used with better performance and a larger pressure range. The generation of a square wave is fairly inexpensive and reliable when compared to the operation of a sine wave generator with high power dissipation. A sine-wave based HF waves usually imply narrow bandwidth whereas square wave generators can easily cover a wide frequency range and large frequency bandwidth.

Fig. 5 shows simulated colour coded efficiency plots as a function of wave amplitude and frequency for the transport of Rb^+ ions. Fig. 5 depicts a larger area of operation for maximum efficiency in Amplitude-Frequency space in the case of the square wave driver.

4. Optimization and a prototype Ion conveyor

In the view of the multiple parameters, which can be varied and tested, some parameters were simply assumed from the technical and manufacturing point of view. Preliminary simulations showed that larger ring electrodes require wave

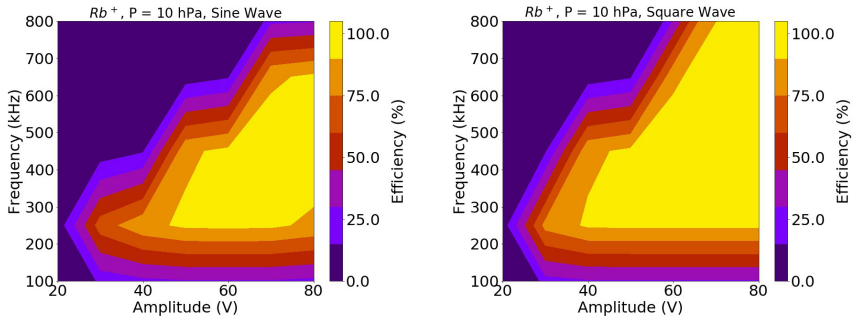

Figure 5: Efficiency plots as a function of wave amplitude and frequency for a conveyor driven by (a) a sinusoidal wave and (b) a square wave. (colour on-line)

amplitudes, that would lead to discharge-limit in Helium. An inner diameter of 10 mm is a reasonable choice to start with. Considering possible parameters and to avoid long computation time, a conveyor length was restricted to the length of 240 mm for the simulation, with a collector at the end. This number also allows for design of structure with even multiplicity in terms of number of rings or inter-electrode distances. The injected ions have a homogeneous spatial distribution in the transverse (x-y) plane without any initial momentum. A gas pressure of 10 hPa was taken as a reference point. The simulations were performed for different structures generated by varying the inter-electrode distance (λ) between ring electrodes while keeping the total length of the structure constant. 8-phases are assumed in all following calculations.

Fig. 6 shows efficiency plots colour coded in the parameter space of wave amplitude and frequency for 4 different structures.

The conveyer shows the highest area representing the maximum transport efficiency of 100% for a distance of $\lambda = 15$ mm. Fig. 7 shows a similar behaviour of the efficiency plots for the Nitrogen$-$ions. In the case of Ar^+ ions, the upper boundary slants down reducing the operational area with high efficiency while

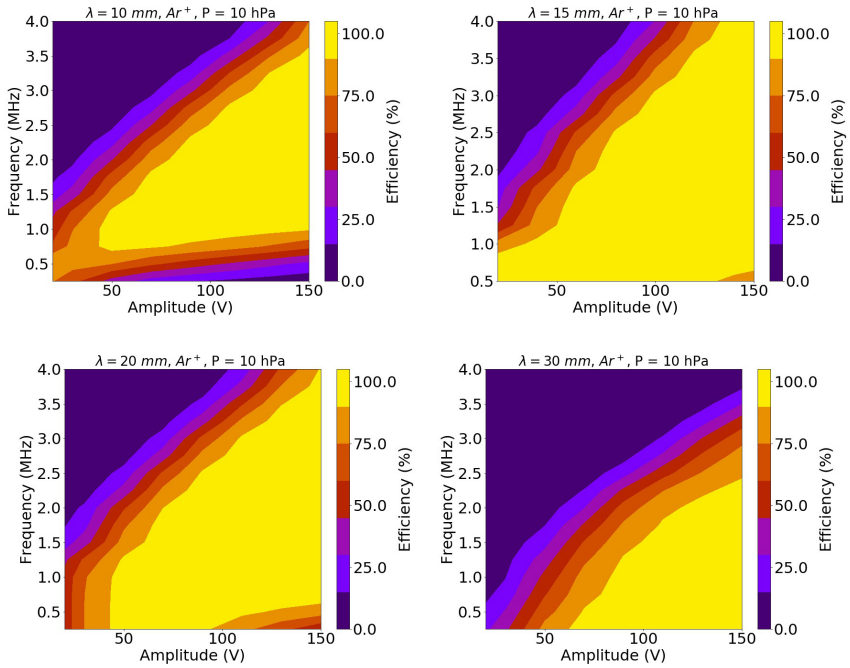

Figure 6: Efficiency plot as a function of wave amplitude and frequency simulated for four different values of distance (λ). Transport of $^{40}Ar^{+}$ ions was simulated through a conveyor with a constant length. (colour on-line)

for the lower mass N^{+} ions this area is shrinking from both sides. The transport of lighter ions is more sensitive to varying period of the structure.

Finally, after fixing the periodic distance at $\lambda = 15$ mm and an inner diameter of 10 mm, one can analyze the performance of the conveyor in terms of pressure range supported.

Fig. 8 shows efficiency plotted for a range of He−gas pressure values and frequencies for heavy ions (Rb^{+}, m = 85) and lighter ions (N^{+}, m = 14) driven at a fixed wave amplitude of 55 V. These graphs show that the structure is well optimized to reach more than 95% efficiency within the pressure range of 7 − 15 hPa for both heavy and lighter ions. It also indicates, in general, a drastic

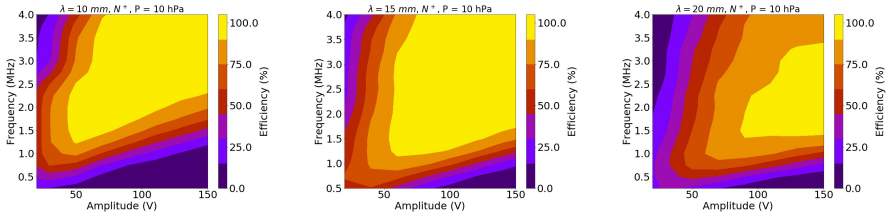

Figure 7: Efficiency plot as a function of wave amplitude and frequency simulated for the transport of N^+ ions. It shows more sensitivity to changing inter-electrode distance. (colour on-line)

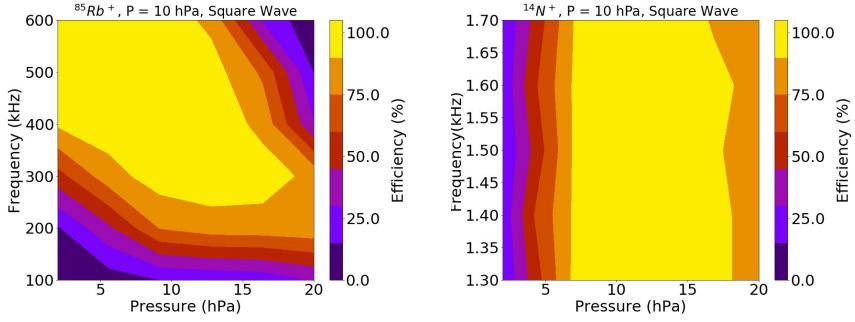

(a) (b)

Figure 8: Pressure range supported by an ion conveyor with a distance of $\lambda = 15$ mm and an inner diameter of 10 mm for the transport of a) heavy ions (Rb^+, m = 85) and b) light ions (N^+, m = 14). (colour on-line)

drop in efficiency on either side of the pressure axis.

The effect of the magnetic field can be included by either importing field distribution from software like TOSCA, EM-STUDIO or it can be taken as an analytical approximation. Fig. 9 shows the simple case of varied magnetic field on the transport of ions through the structure for heavier and lighter ion types. The difference in the transport efficiency is very small within an error limit in both the case when the magnetic field is applied.

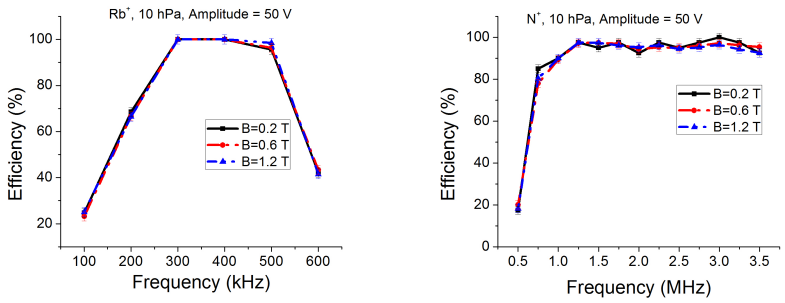

(a) (b)

Figure 9: Effect of magnetic field on the efficiency of ion transport through the structure for two different cases of a) Rb^+, m = 85 ions and b) N^+, m = 14 ions. (colour on-line)

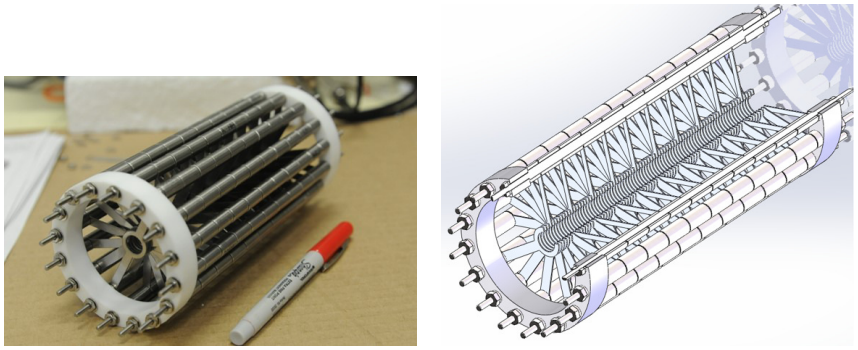

(a) (b)

Figure 10: The tested prototype Ion Conveyor a) a photograph and b) CAD drawing with a quarter removed to show the inside.

A test ion conveyor has been built based on these values for demonstration experiments. The device is constructed with 80 electrodes, with a consecutive electrode spacing of 1.875 mm or a spacer length 15 mm supporting 8−phases as shown in Fig. 10. The total length of the conveyor is 180 mm. Double-spoke electrodes are mounted in staircase pattern into 16 rods held in place by

Macor rings. The whole assembly was then inserted into a cylindrical vessel with electrical isolation from electrodes. An additional collimator plate in the front and a collector plate downstream were attached for experiments. The construction of the mounting assembly is matched in order to use existing the experimental facility.

5. Experiments

Fig. 11 shows a SIMION depiction of the experimental setup. A surface ion source was mounted in front of the ion conveyor. For the transport of heavier isotopes, an $^{85}Rb^{+}$ emitting ion source was used. A high-quality pellet surface ion source provides $^{85}Rb^{+}$ ions up to 92% measured using RGA scanner. The collimator plate provides better control of ion injection into the ring structure. The collector at the end was connected to a picoampere meter. Helium was used as buffer gas for all the experiments.

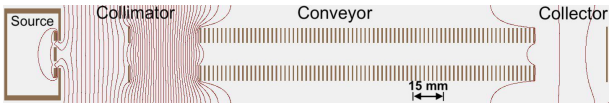

Figure 11: Experimental setup showing ion source, collimator, ion conveyor and collector. This is a typical SIMION depiction with equipotential lines. A scale of 15 mm corresponding to spacer length is shown.

Fig. 12 shows efficiency as a function of the buffer gas pressure. Fig. 12(a) show efficiency measured at frequency 250 kHz with a wave amplitude of 40 V. The simulation predicts a constant efficiency of 100% above 5 hPa whereas the measured efficiency drops down slowly above 8 hPa. In the second graph, seen in Fig. 12(b), the measured values agree better with the simulated values when the structure is driven at 300 kHz and a wave amplitude of 45 V. However, both the graphs indicate a sharp efficiency drop below 3 hPa as predicted by simulations.

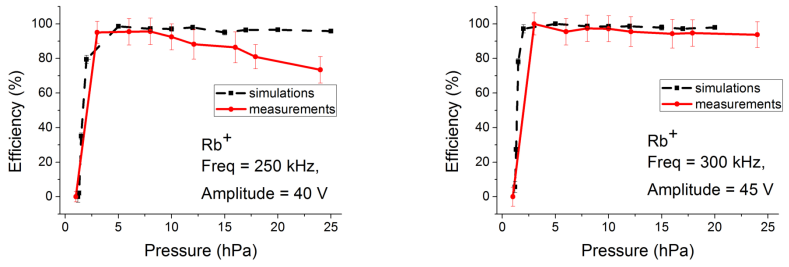

(a) (b)

Figure 12: Measured and simulated efficiency as a function of gas pressure for the transport of $^{85}Rb^{+}$ ions at a) f = 250 kHz, and at (b) f = 300 kHz.

Fig. 13 gives a more comprehensive view of this comparison. The efficiency is plotted in the amplitude-frequency space for the transport of Rb^{+} ions in the presence of a gas pressure of 10 hPa. At lower amplitudes, the simulated values do not match with measurements exactly. The measurements show a slower rise in efficiency than simulations with increasing wave amplitudes. Both graphs show little change in efficiency as a function of the amplitude. The overall behaviour of the measured efficiency function is qualitatively similar to the simulated one.

The performance of the ion conveyor was also tested for lower mass ions, e.g. a $^{23}Na^{+}$. As the $^{23}Na^{+}$ source was not able to deliver a stable ion beam for the time needed to cover the desired full Amplitude-Frequency range, only a subset of measurements was taken.

Fig. 14 shows a graph of efficiency as a function of frequency for the transport of Na^{+} ions with a wave amplitude of 50 V in the presence of the gas pressure of 10 hPa. The measured efficiency curve rises slowly, reaching a maximum of about 98% before slowly decreasing again, whereas the simulated values stay constant at 100% for frequencies values over 600 kHz.

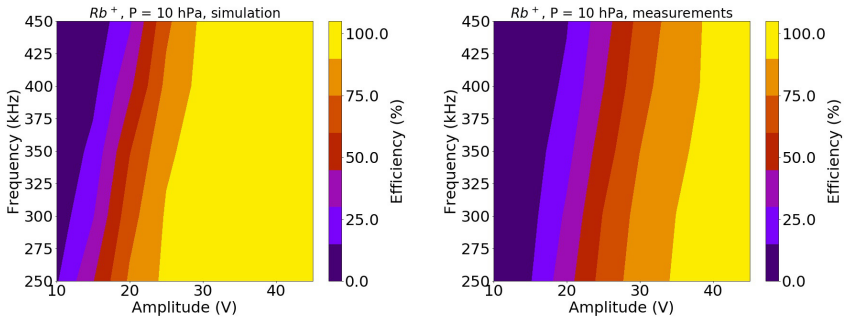

(a) (b)

Figure 13: Simulated and measured efficiency as a function of wave amplitude and frequency for the transport of Rb^+ ion at 10 hPa. (colour on-line)

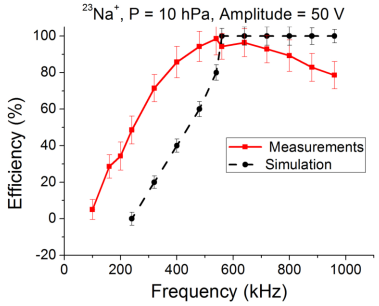

Figure 14: Efficiency as a function of frequency showing the comparison between simulations and measurements.

6. Conclusions

The demonstration experiments show that the ion conveyor with a scaled version (L = 180 mm) can transport heavy ions (Rb^+) and lighter ions (Na^+) with very good efficiency. In the case of Rb^+ ions, about $100 \pm 3.2\%$ efficiency was achieved, whereas Na^+ ions were measured with $97.8 \pm 8.1\%$ efficiency. The measurements and simulations are shown in good agreement with a tolerable

error margin for Rb^+ ions at higher frequency and amplitude. Although in many cases e.g. at lower amplitudes, the measurements do not match with the simulations, the qualitative behaviour of the efficiency dependence on the parameters is similar. The prototype constructed for demonstration experiments was only 180 mm in length.

To investigate scalability of the structure , the distribution of lost ions along the conveyor was simulated for the transport of Ar^+ driven at 400 kHz. Fig. 15 shows the simulated histogram of lost ions as a function of distance along the longitudinal axis of the conveyor.

Fig. 15(a) shows the distribution of lost ions for different wave amplitude over the distances, whereas Fig. 15(b) shows a similar distribution at different pressure values.

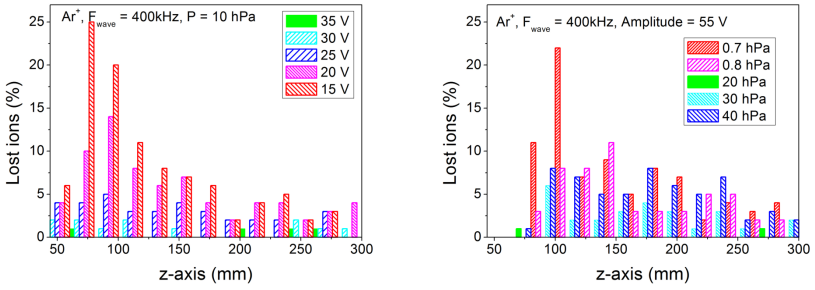

(a) (b)

Figure 15: Distribution of lost ions along the conveyor for transport of Ar^+ ions. a) Distribution as a function of distance for different wave amplitudes at 10 hPa. b) Distribution of lost ions as a function of distance for different pressure values with a wave amplitude of 55 V.

These graphs show that there are significant losses at low amplitude, and the lower pressure end. With sufficiently high wave amplitudes > 30 V and pressure above 7 hPa, the losses are constant and very low along the structure. Thus a longer ion conveyor is expected to support efficient ion transport even with some expected pressure gradient in the range of $7 - 12$ hPa along the channel.

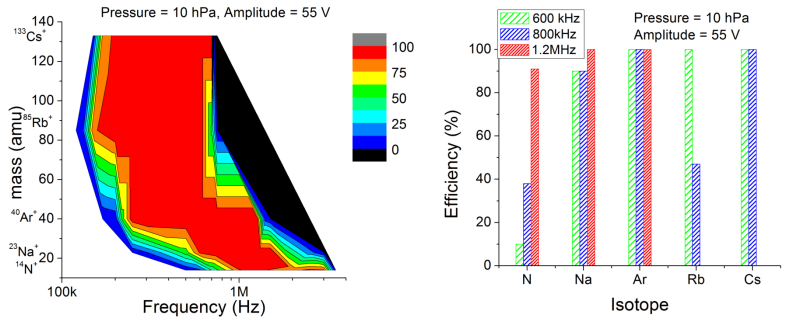

Figure 16: Efficiency diagram showing the operational frequency space for different ion masses at a fixed amplitude of 55 V (colour on-line) and efficiencies shown in a bar chart for few chosen isotopes in the presence of buffer gas pressure of 10 hPa.

Fig. 16 shows an efficiency plot for different masses and frequency range at a fixed wave amplitude of 55 V and a gas pressure of 10 hPa. As displayed in the representative bar graph, the heavier ions can be extracted within a lower frequency range of about $300 - 450$ kHz and lighter ions require higher frequencies around $2 - 4$ MHz. This plot can be used as a reference for a wide range of radioactive beam which will be produced at the facility. Table 1 summarizes a few parameters for selected range of ions.

Table 1: Typical values for different ions for more than 80% transport efficiency.

Ion	Minimum Voltage at Optimum Frequency	Frequency Range	Amplitude Range	Pressure Range
$^{133}Cs^{+}$	35 V @250 kHz	$200 - 400$ kHz	$50 - 70$ V	$5 - 20$ hPa
$^{85}Rb^{+}$	35 V @250 kHz	$200 - 400$ kHz	$50 - 70$ V	$7 - 20$ hPa
$^{40}Ar^{+}$	35 V @400 kHz	$400 - 700$ kHz	$50 - 60$ V	$7 - 20$ hPa
$^{23}Na^{+}$	35 V @600 kHz	$600 - 1000$ kHz	$50 - 70$ V	$7 - 20$ hPa
$^{14}N^{+}$	50 V @1.5 MHz	$2 - 3.5$ MHz	$55 - 70$ V	$6 - 12$ hPa

7. Acknowledgement

The authors would like to acknowledge G. Bollen, S. Schwarz, D. Morrissey and R. Ringle for participation in the discussions and guidance.

Appendix A. Square Wave Generator

A travelling wave can be generated by producing multiple periodic signals, shifted by equal phases. In the case of a sinusoidal wave, it can be achieved by a combination of OpAmps connected in Adder and Subtractor circuit with an additional phase difference. A square wave generator was shown to be a better solution and also a more economical one than a sinusoidal wave generator. A single channel square signal is generated using MOSFET in push-pull configuration. Fig. A.17 shows a basic circuit of a square wave generator using two MOSFETs, one with p-channel and other with n-channel.

The circuit is mounted on a good conducting metal plate with additional capacitors to reduce the ringing effect.

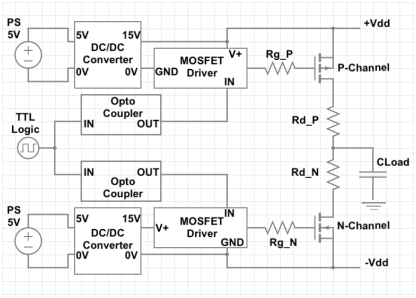

Figure A.17: Two MOSFETs in push-pull configuration generates a square wave.

The MOSFETs, IRF630 and IRF9630, exhibits a typical output capacitance of 89 pF and 200 pF respectively. This combination can be used to achieve a rise time and fall time of about 240 ns with a load of 20 pF, whereas it increases up to 500 ns with an increased load of 800 pF. These values were almost stable over the frequency range of 200 kHz – 1.2 MHz. Fig. A.18 shows a square wave

with an amplitude of 50 V at 200 kHz. The ringing effect shows an overshoot and undershoots in the voltage of about 8 V. This voltage fluctuation does not affect the ion transport within the tolerance.

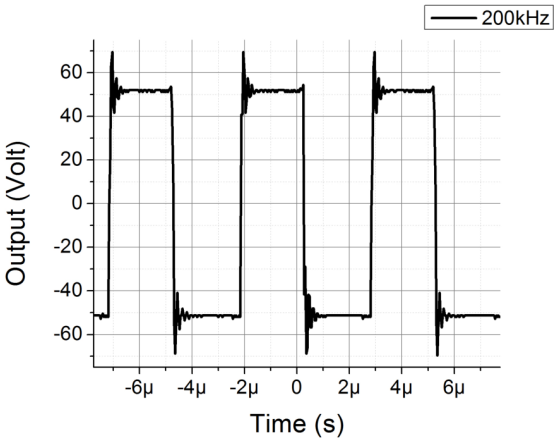

Figure A.18: Measured single-channel squarewave at 200 kHz.

Eight such channels have been designed and manufactured. The travelling wave can be produced by introducing a phase shift in consecutive output channels. For this purpose, we employ a combination of octal counter and the flip-flops to drive the TTL-logic of each channel at different phases. Fig. A.19 shows the oscilloscope output of the driving clock signal and the first four channels, indicating the phase shift.

References

[1] R. Bahr, D. Gerlich, and E. Teloy (1969), Verhandl. DPG (V I) 4, 343.

[2] Shenheng Guan, Alan G.Marshall, "Stacked-ring electrostatic ion guide", Journal of the American Society for Mass Spectrometry, (1996) Volume 7, Issue 1, 101-106.

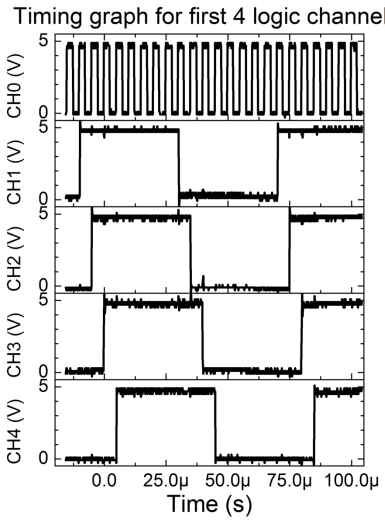

Figure A.19: Oscilloscope output of the driving clock signals and phase-shifted signals provided to TTL-logic of the MOSFET.

[3] Richard D. Smith et al., "An Ion Funnel Interface for Improved Ion Focusing and Sensitivity Using Electrospray Ionization Mass Spectrometry ", Anal. Chem. (1998), 70, 4111-4119.

[4] Richard D. Smith et al., "Design and Implementation of a New Electrodynamic Ion Funnel", Anal. Chem. (2000), 72, 2247-2255.

[5] Richard D. Smith et al., "The Ion Funnel: Theory, Implementations, and Applications", Mass Spectrom. Rev. (2010) 29(2).

[6] Alex W. Colburn, A.E. Giannakopulos and Peter J. Derrick, "The Ion Conveyor. An ion focusing and conveying device", Eur. J. Mass Spectrom. (2004), 10, 149-154.

[7] M. Brodeur, N. Joshi, A.E. Gehring, G. Bollen, D.J. Morrissey, S. Schwarz, "Traveling wave ion transport for the cyclotron gas stopper", Nuclear In-

struments and Methods in Physics Research B, Volume 317, Part B, 15 December 2013, Pages 468-472.

[8] Michiharu Wada et al, "Slow RI-beams from projectile fragment separators", Nuclear Instruments and Methods in Physics Research B 204 (2003) 570-581.

[9] G. Bollen, " "Ion surfing" with radiofrequency carpets ", International Journal of Mass Spectrometry Volume 299, Issues 2?3, 15 January 2011, Pages 131-138.

[10] M. Brodeur, A.E. Gehring, G. Bollen, S. Schwarz, D.J. Morrissey, "Experimental investigation of the ion surfing transport method", International Journal of Mass Spectrometry, Volume 336, 15 February 2013, Pages 53-60.

[11] A.E. Gehring, M. Brodeur, G. Bollen, D.J. Morrissey, S. Schwarz, "Research and development of ion surfing RF carpets for the cyclotron gas stopper at the NSCL", Nuclear Instruments and Methods in Physics Research B 376 (2016) 221-224.

[12] D. Manura, D. Dahl. SIMION (R) 8.0 User Manual, Scientific Instrument Services, Inc. Ringoes, NJ 0855, http://simion.com , January 2008.

[13] S. Schwarz, "IonCool-A versatile code to characterize gas-filled ion bunchers and coolers (not only) for nuclear physics applications", Nuclear Instruments and Methods in Physics Research A, 566 (2006), 233-243.